P. Masarati, G. Quaranta
Bioaeroservoelastic Analysis of Involuntary Rotorcraft-Pilot Interaction
Journal of Computational and Nonlinear Dynamics, Vol. 9, N. 3, 2014, 031009 (9 pages)
doi:10.1115/1.4025354

Bioaeroservoelastic Analysis of Involuntary Rotorcraft-Pilot Interaction

Pierangelo Masarati[*], **Giuseppe Quaranta**
Politecnico di Milano, Dipartimento di Scienze e Tecnologie Aerospaziali
mail: {pierangelo.masarati,giuseppe.quaranta}@polimi.it

This work presents the integration of a detailed biomechanical model of the arms of a helicopter pilot and an equivalently detailed aeroservoelastic model of a helicopter, resulting in what has been called a 'bioaeroservoelastic' analysis. The purpose is to investigate potential adverse interactions, called rotorcraft-pilot couplings, between the aeroservoelastic system and the controls involuntarily introduced by the pilot into the control system in response to rotorcraft vibrations transmitted to the pilot through the cockpit, the so-called biodynamic feedthrough. The force exerted by the pilot on the controls results from the activation of the muscles of the arms according to specific patterns. The reference muscular activation value as a function of the prescribed action on the controls is computed using an inverse kinetostatics/inverse dynamics approach. A first-order quasi-steady correction is adopted to mimic the reflexive contribution to muscle activation. Muscular activation is further augmented by activation patterns that produce elementary actions on the control inceptors. These muscular activation patterns, inferred using perturbation analysis, are applied to control the aircraft through the pilot's limbs. The resulting biomechanical pilot model is applied to the aeroservoelastic analysis of a helicopter model expressly developed within the same multibody modeling environment to investigate adverse rotorcraft pilot couplings. The model consists of the detailed aeroelastic model of the main rotor, using nonlinear beams and blade element/momentum theory aerodynamics, a component mode synthesis model of the airframe structural dynamics, and servoactuator dynamics. Results in terms of stability analysis of the coupled system are presented in comparison with analogous results obtained using biodynamic feedthrough transfer functions identified from experimental data.

[*]Corresponding author: Politecnico di Milano, Dipartimento di Scienze e Tecnologie Aerospaziali, via La Masa 34, 20156 Milano, Italy

1 INTRODUCTION

This work presents the application of an approach initially developed for the inverse dynamics analysis and characterization of the upper limbs of human operators [1, 2]. The approach was applied to the characterization of the left arm of helicopter pilots acting on the collective control inceptor. It is based on the inverse kinetostatics/inverse dynamics analysis of a detailed biomechanical model implemented using MBDyn (`http://www.mbdyn.org/`), a free general-purpose multibody analysis software.

Biodynamic feedthrough (BDFT, [3]) results in commands involuntarily produced by pilots as a consequence of vibrations of the cockpit acting on their body. This problem is of utmost interest for the investigation of aeroelastic Rotorcraft-Pilot Couplings, i.e. the interaction between the aeromechanics of the vehicle and controls inadvertently generated by pilots.

The problem has been extensively analyzed with reference to fixed-wing aircraft, both in terms of intentional (Pilot-Induced Oscillations, PIO) and passive interaction (Pilot-Augmented Oscillations, PAO) [4], while helicopters received less attention, especially with respect to PAO [5]. The latter are characterized by frequencies in the range of 2–8 Hz, which are too high to be intentionally tracked and controlled by pilots. However, fundamental biomechanical frequencies fall in this band, as well as typical aeroservoelastic modes of fixed and rotary wing aircraft.

Current practice consists in using simplified models of the pilot's BDFT within the aeroservoelastic analysis of the vehicle [6]. Simple pilot models consist of transfer functions identified from experiments based on cockpit mock-ups, flight simulators or actual aircraft [7–10]. Such an approach is limited by the need to test actual cockpit layouts, considering several aspects like variability of human operators, workload dependence, learning effects.

The proposed approach consists in modeling the in-

ASME J. Comput. Nonlinear Dyn. MONTH YYYY V(N), doi:10.1115/DDDDDDDDD

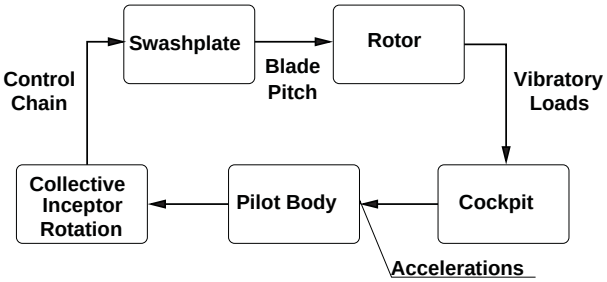

Fig. 1. Block scheme of vertical bounce feedback loop between pilot biomechanics and rotor aeromechanics.

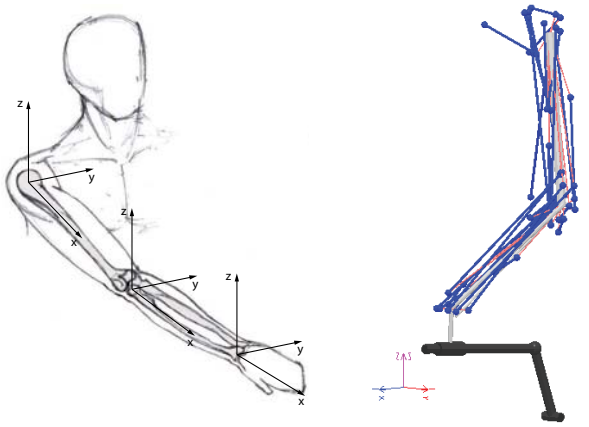

Fig. 2. Multibody model of the arm holding the collective control inceptor.

voluntary biomechanics of the pilot in the desired reference configurations using the multibody dynamics approach, with muscle constitutive properties derived from Hill-type models. The models are used to perform virtual experiments to understand the variability of neuromuscular admittance (NMA) and BDFT in realistic operating conditions.

The approach proposed in [1, 2] can be viewed as overly deterministic, considering the variability of the properties of human subjects characteristic of biomechanics. Such properties depend not only on general characteristics like the size, the weight, the conditions of each limb, articulation and muscle, but also on the level of muscular activation of the muscles themselves. The muscular activation depends on the task, the level of attention, workload, training and other subjective, random or hardly quantifiable parameters.

The analysis in [1, 2] consists of a sequence of steps. First, the kinematics of the task are reconstructed using a kinetostatic analysis, in which an 'optimal' position and trajectory of the underdetermined limbs is computed as a function of the trajectory prescribed to the hand. Underdetermination is cured using relatively arbitrary ergonomy functions, although the output of a motion capture system could be used as well, as proposed for example in [11–15]. In a subsequent phase, the corresponding inverse dynamics problem is solved, to determine the torques in the articulations, and the corresponding muscular activation levels are computed according to minimal activation norm.

In this work, the resulting biomechanical model is applied for the first time to the direct simulation of adverse Rotorcraft-Pilot Coupling (RPC) problems, specifically addressing the collective bounce phenomenon. In some conditions, vibratory loads generated by the rotor can cause vertical accelerations of the cockpit. Such accelerations, transmitted through the pilot's body to the rotor collective pitch control lever, send oscillating signals to the swashplate, thus causing a collective variation of blade pitch that may cause further vibratory loads. The involuntary feedback loop is shown in Fig. 1.

First, the isolated arm holding the collective control inceptor is used to determine the NMA and the BDFT of the pilot associated to that control device. Direct integration in time is performed under harmonic excitation; the results are analyzed to produce the related plots.

Subsequently, the multibody model of the arm and of the control inceptor is added to a previously developed detailed multibody aeroservoelastic model of a medium weight helicopter [16]. Coupled analyses are presented, in which the interaction is parametrized considering the gearing ratio between the rotation of the control device and the actual main rotor blade pitch change.

2 BIOMECHANICAL MODEL OF THE PILOT'S ARM

A multibody model of the left arm has been implemented (Fig. 2). The model consists of rigid bodies connected by ideal kinematic constraints. The arm is grounded at the shoulder. The humerus, the radius, the ulna and the hand are modeled as rigid bodies, accounting for $6 \times 4 = 24$ degrees of freedom. The hand has not been detailed because the work focuses on tasks that require an inceptor to be firmly grasped.

The articulation of the shoulder complex is modeled as a spherical hinge that prescribes the coincidence of the center of the proximal condyle of the humerus and the center of the glenoidal fossa. As a consequence, 3 degrees of freedom are removed. A revolute hinge, which approximates the humeroulnar joint, allows the rotation of the ulna with respect to the humerus, about the *y*-axis of the ulna itself. The axis is centered in the trochlea. As a consequence, 5 more degrees of freedom are removed. The humeroradial joint is approximated by a spherical joint that prescribes the center of the capitulum to be in a point slightly outside the physical proximal end of the radius,

ASME J. Comput. Nonlinear Dyn. MONTH YYYY V(N), doi:10.1115/DDDDDDDDD

Table 1. Geometry and inertia properties of the arm's bodies.

Body mass	70	kg			
Height	170	cm			
	length	mass	J_{xx}	J_{yy}	J_{zz}
	mm	kg	kg·mm^2	kg·mm^2	kg·mm^2
Humerus	297	2.02	2555.2	14411.2	16228.9
Radius	261	0.61	388.2	2662.0	2717.0
Ulna	261	0.59	582.2	3994.0	4076.0
Hand	68	0.43	195.4	724.0	724.0

thus removing 3 more degrees of freedom. The proximal and distal radioulnar joints are approximated using a single inline joint between a point P and the mechanical x-axis of the ulna. The point P is offset from the radius axis in the local y direction, in such a manner that the two bones are parallel in rest position (more details can be found in [17]). Such position is defined as the configuration in which the arm is completely extended, pointing anteriorly, with the palm facing upward. The inline joint removes 2 degrees of freedom. A universal hinge models the carpal complex, thus allowing the flexion and the radio-ulnar deviation of the wrist, removing 4 more degrees of freedom. The resulting model has 7 degrees of freedom, and would thus be underdetermined even if the motion of the hand were completely prescribed. The geometry and the inertia properties of the model are reported in Table 1. They refer to a person of about 170 cm height and 70 kg weight.

The muscles (a complete list is reported in Table 2) are modeled using the simplified Hill model proposed in [17]. The force exerted by the muscle is

$$f = f_0 \left(f_1(x) f_2(v) a + f_3(x) \right), \tag{1}$$

where f_0 is the peak isometric force, $x = l/l_0$ and $v = \dot{l}/v_0$ are the normalized length and elongation rate of the muscle, and $0 \leq a \leq 1$ is the activation parameter. Functions f_1, f_2 and f_3 are illustrated in Fig. 3. According to the literature (see [17]), the compliance of the tendons is sufficiently low with respect to that of the non-activated muscles to be negligible; function f_3 approximates the elastic behavior of the tendons when l exceeds the non-activated muscle length, l_0. The model does not account for variations in muscle mass distribution during contraction and extension; such an approximation is not considered critical in the case under analysis. Figure 4 presents the muscular activation level, a, at 10%, 50%, and 90% reference collective position for the muscles listed in Table 2.

The reflexive contribution to activation described in [18,19] to explain the higher total equivalent stiffness and damping of muscles compared to their intrinsic (i.e. passive) value is modeled using a quasi-steady approximation,

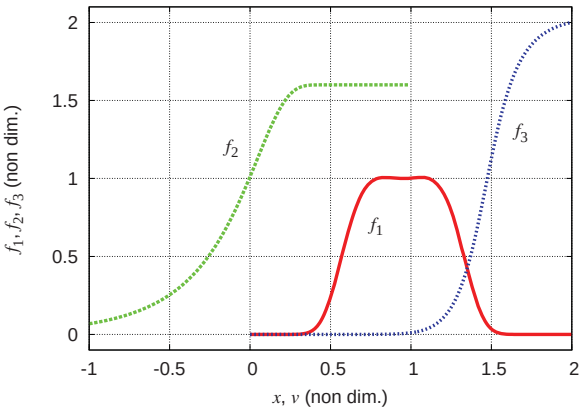

Fig. 3. Non-dimensional functions used in Eq. (1).

$$\Delta a = K_p \Delta x + K_d \Delta v, \tag{2}$$

such that force perturbations can be expressed as

$$\begin{aligned} \Delta f = f_0 \big(\big(\big(f_{1/x} a + f_1 K_p \big) f_2 + f_{3/x} \big) \Delta x \\ + f_1 \left(f_{2/v} a + f_2 K_d \right) \Delta v \big) . \end{aligned} \tag{3}$$

Values of K_p = 0.8 and K_d = 0.3 have been estimated from the ratios of total and intrinsic stiffness and damping from [18].

According to Fig. 4, different reference positions require different muscular activation levels; considering the impact of activation on the muscle force perturbation of Eq. (3), this implies different equivalent compliance values.

Three tasks representative of typical pilot activity are considered. They are derived from the experiments performed in [3]. In that experiment, pilots were asked to perform

PT: a *position task*, consisting in keeping the control inceptor in a prescribed position as accurately as possible, resisting forces;

RT: a *relax task*, consisting in loosely keeping the control inceptor about a prescribed position;

FT: a *force task*, consisting in yielding to forces without trying to keep the inceptor in a specific position.

Each task is conjectured to require human operators attain specific neuromuscular settings, consisting in different levels and combinations of muscular activation. The PT is expected to require a significant amount of reflexive activation on top of a minimal reference activation, essentially required to counteract the own weight of the arm. This behavior is produced in the model by using a high level of reflexive proportional gain K_p (the nominal value 0.8 mentioned earlier), on top of the baseline activation

Table 2. Arm muscles' properties: reference length (l_0); max isometric force (f_0); coordinates of insertion points 1 & 2 (x_1 & x_2).

		l_0	f_0	x_1	y_1	z_1	x_2	y_2	z_2
		mm	N	mm	mm	mm	mm	mm	mm
Muscles connecting humerus to the rest of the body									
1	Coracobrachialis	197	242.5	20	30	35	174	21	0
2	Deltoid — anterior fascicles	179	1142.6	35	25	35	136	-12	10
3	Deltoid — middle fascicles	159	1142.6	35	-22	20	136	-24	18
4	Deltoid — posterior fascicles	148	259.9	-35	10	0	136	-24	18
5	Latissimus dorsi	380	1059.2	-65	110	-290	75	25	9
6	Pectoralis major	147	1270.3	45	110	10	36	0	25
7	Supraspinatus	108	487.8	-36	80	35	-32	2	-13
8	Infraspinatus	111	1210.8	-32	80	-40	-26	0	-20
Muscles connecting radius to the rest of the body									
9	Biceps brachii caput longus	388	624.3	0	-15	10	34	16	0
10	Biceps brachii caput brevis	324	435.6	20	30	25	3	16	0
Muscles connecting ulna to the rest of the body									
11	Triceps brachii caput longus	290	798.5	-35	20	-20	-15	0	-22
Muscles connecting humerus to ulna									
12	Anconeus	55	350.0	300	-5	-12	-14	7	-11
13	Triceps brachii caput laterale/mediale	211	1248.6	112	0	-28	-27	0	-6
14	Brachialis	140	987.3	196	-8	16	17	15	5
Muscles connecting humerus to radius									
15	Brachioradialis	306	261.3	246	-7	0	238	-18	13
16	Pronator teres	148	566.2	270	33	-7	55	-18	12
Muscles connecting humerus to hand									
17	Flexor carpi ulnaris	317	128.9	265	27	-5	5	30	23
18	Extensor carpi ulnaris	290	93.2	269	-27	-5	5	30	-18
19	Extensor digitorum	387	100.7	269	-20	-20	8	0	-16
20	Flexor digitorum superficialis	380	226.6	275	27	-10	7	18	26
21	Flexor carpi radialis	307	74.0	275	27	-7	3	-20	32
22	Extensor carpi radialis	305	405.4	245	-20	0	5	-23	-11
Muscles connecting ulna to radius									
23	Pronator quadratus	33	75.5	200	7	14	236	27	23
24	Supinator	61	476.0	13	17	-8	28	13	-24
Muscle connecting ulna to hand									
25	Abductor pollicis longus	202	59.5	115	-21	-5	3	-18	23

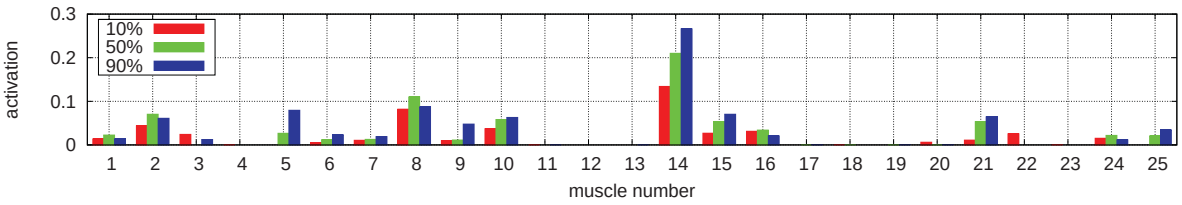

Fig. 4. Muscular activation levels for 10%, 50% and 90% collective control device reference position (muscle numbers from Table 2).

computed for each arm configuration. The FT is obtained by setting the reflexive activation gain to zero, while the RT is obtained by setting the reflexive activation gain to an intermediate level (K_p = 0.2 was used in the analysis).

As an additional source of perturbation, activation levels required to counteract a steady torque applied to the collective control inceptor have been considered, yielding a non-minimal reference activation condition.

2.1 Collective Control Biodynamic Feedthrough

The BDFT, i.e. the rotation of the control inceptor as a function of the acceleration of the cockpit, has been evaluated by exciting the pilot's arm model with a pre-

scribed harmonic motion of the seat in the surge, sway and heave directions. The bode plots of the BDFT related to the collective control for heave are shown in Fig. 5. The plots on the left compare the BDFT resulting from the three tasks (PT, RT, FT) at 10%, 50%, and 90% reference collective position. Significant task dependence can be appreciated, in line with that experimentally determined in [3] although for a different layout of the control device. Specifically, higher reflexive gain tasks present the dominant biomechanical poles with a higher frequency. The plots on the right compare the BDFT at 10%, 50%, and 90% reference collective position for each of the three tasks (PT, RT, FT). A clear dependence on the reference control position can be appreciated as well, in line with the discussion in [7] and with the results of the experiments presented in [9], where tasks equivalent to the PT yielded a frequency of the dominant poles that decreased with increasing reference position of the control device.

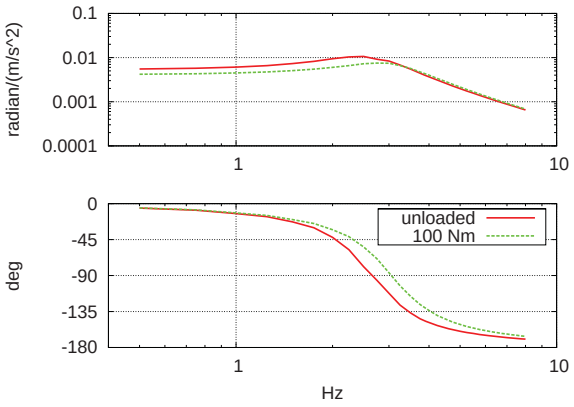

Fig. 7. Comparison of collective control BDFT between an unloaded inceptor and one loaded with a steady 100 N·m torque (position task, 50% reference collective rotation, harmonic excitation).

2.2 Collective Control Neuromuscular Admittance

The NMA associated with the collective control inceptor, i.e. the rotation of the collective control inceptor as a function of a torque applied to the inceptor itself, has been evaluated by prescribing the harmonic rotation of the collective control to excite the pilot's arm, and by analyzing the corresponding constraint reaction. The bode plots of the NMA related to the collective control for heave are shown in Fig. 6. The plots on the left compare the NMA resulting from the three tasks (PT, RT, FT) at 10%, 50%, and 90% reference collective position. As already noted for the BDFT, significant task dependence can be appreciated, in line with that experimentally determined in [3]. Specifically, higher reflexive gain tasks present the dominant biomechanical poles with a higher frequency. The plots on the right compare the NMA at 10%, 50%, and 90% reference collective position for each of the three tasks (PT, RT, FT). A clear dependence on the reference control position can be appreciated as well.

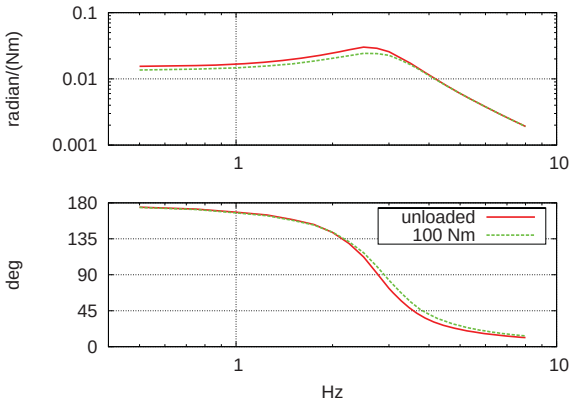

Fig. 8. Comparison of collective control NMA between an unloaded inceptor and one loaded with a steady 100 N·m torque (position task, 50% reference collective rotation, harmonic excitation).

2.3 BDFT and NMA Under Load

The BDFT and the NMA of the pilot while requested to counteract a steady 100 N·m torque applied to the collective control are shown in Figs. 7 and 8. The need to counteract the load causes additional muscular activation, which increases the equivalent stiffness of the muscles. As a consequence, BDFT and NMA are generally lower than in the reference condition, while the poles shift toward a higher frequency.

2.4 Use of NMA and BDFT

The availability of the results presented in the previous sections is very important for practical applications. The Bode plots of the BDFT can be directly used to evaluate the robustness of the stability and of the performances of pilot-in-loop vehicle models, even in graphical form, as proposed in [20, 21]. Figures 9 and 10 present the envelopes of BDFT and NMA Bode plots, obtained by determining the extremal values of all the estimated frequency responses.

Transfer functions can be identified from the numerical BDFT and NMA data, to be used in linear/linearized analysis [5, 6]. Transfer functions identified from BDFT can be directly used in aeroservoelastic simulations by closing the vehicle control loop: consider for example the pilot BDFT relation

$$\psi = H_{\mathrm{BDFT}}(s)\ddot{z}, \tag{4}$$

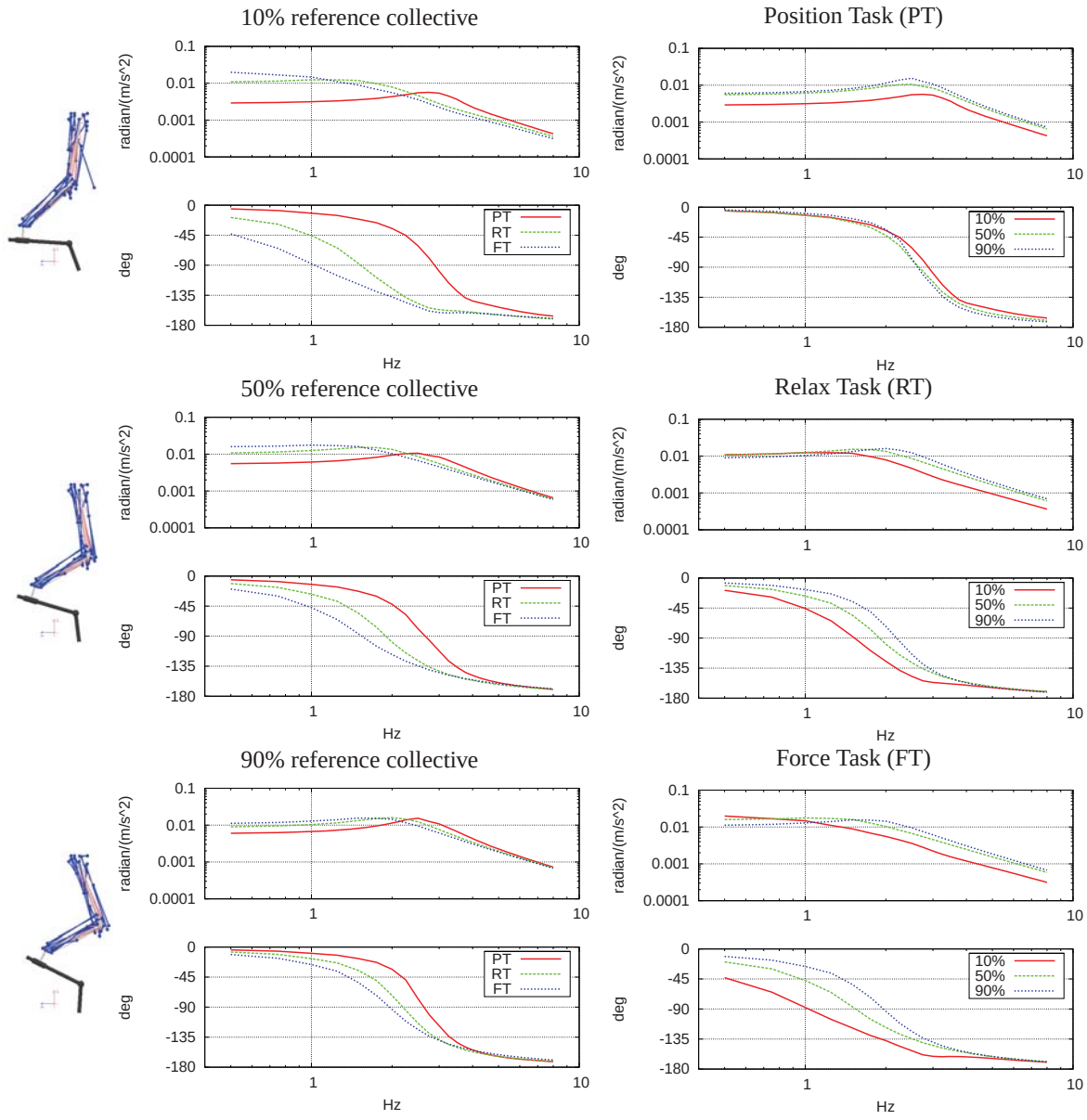

Fig. 5. Collective control BDFT (harmonic excitation).

where ψ is the control device rotation and z is the heave motion of the cockpit. An aeroservoelastic model of the vehicle

$$z = H_{z\theta}(s)\theta_0 + H_{zu}(s)u \tag{5}$$

expresses z as a function of the collective pitch θ_0 and of u, a generic input/disturbance (e.g. a gust). The coupled problem is

$$\left(1 - H_{z\theta}(s)GG_cH_{\mathrm{BDFT}}(s)s^2\right)z = H_{zu}(s)u, \tag{6}$$

where GG_c is the gearing ratio between the control inceptor rotation and the collective pitch, $\theta_0 = GG_c\psi$ (G_c is the nominal value, while the scaling factor G is used later as a parameter to study the sensitivity of the coupled system dynamics to BDFT).

When a NMA function $\psi = H_{NMA}(s)m$ is available, where m is the moment applied to the control device, the dynamics of the control device can be accounted for. The control device rotation can be expressed as

$$\psi = H_{NMA}(s)m + H_{\mathrm{BDFT}}(s)\ddot{z}; \tag{7}$$

the moment can be expressed as

$$m = H_{NMA}^{-1}(s)\left(\psi - H_{\mathrm{BDFT}}(s)\ddot{z}\right). \tag{8}$$

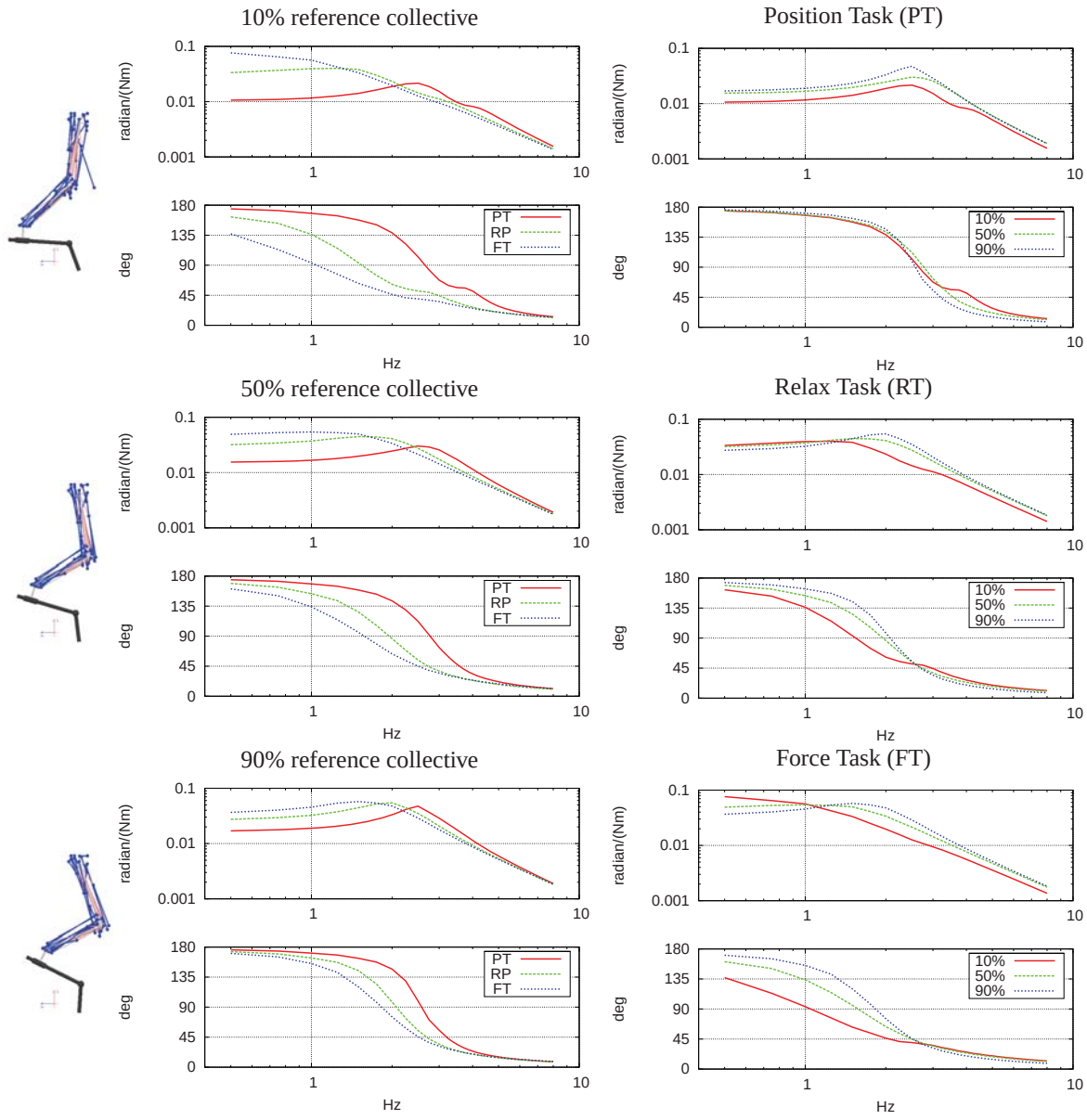

Fig. 6. Collective control NMA (harmonic excitation).

Laplace transform manipulation can be used to express the moment m, involuntarily applied by the pilot to the control inceptor, as a function of ψ and z and their time derivatives also in the time domain, and thus to write the equations of motion of the control inceptor. This aspect of the analysis is currently under development.

3 ROTORCRAFT MODEL

A detailed aeroservoelastic model of a medium weight helicopter, based on data from the Sud-Aviation (now Eurocopter) SA330 Puma, has been developed for the analysis of rotorcraft-pilot couplings using the general-purpose multibody solver MBDyn and correlated in terms of stability and response with a corresponding linearized model obtained using comprehensive aeroelastic rotorcraft analysis tools [16].

The multibody model consists of the subsystems that have been observed to be essential for the simulation of the vertical bounce phenomenon [6, 22–24]: a detailed aeroelastic model of the main rotor, the aeromechanics equations associated with heave and yaw, the structural dynamics of the airframe, and a model of the control system that accounts for the dynamics of the swashplate actuators.

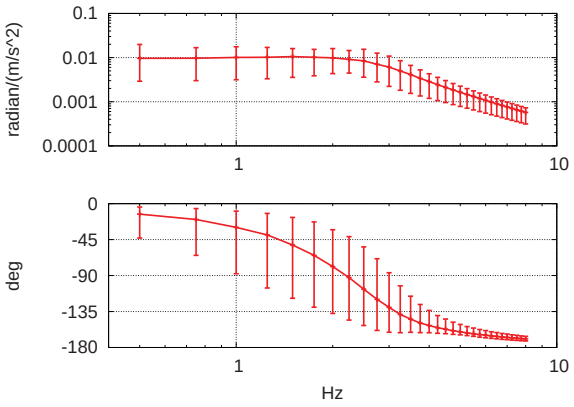

Fig. 9. Envelope of collective control BDFT.

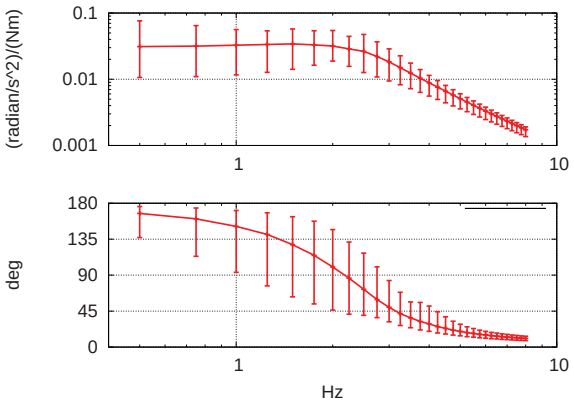

Fig. 10. Envelope of collective control NMA.

The aeroelasticity of the main rotor is modeled using 5 three-node nonlinear beam elements for each blade; lumped deformable elements model the hydraulic lead-lag dampers and the pitch links, and ideal joints model the kinematics of the hub and blade articulations. Detailed rotor aeroelastic data were taken from [25]. The aerodynamic model is based on the blade element theory, with induced velocity based on the momentum theory and accounted for using the dynamic inflow model proposed by Pitt and Peters [26]. The rigid-body motion of the airframe and its structural dynamics are modeled using a modal joint element essentially based on the component mode synthesis approach. Eight normal modes involving appreciable modal participation of the main rotor attachment point and of the pilot's seat have been used; the largest frequency was about 20 Hz. A set of first-order transfer functions with cutoff frequency of about 10 Hz is used to approximate the dynamics of the swashplate actuators. The overall model consists of about 900 differential-algebraic equations. The angular velocity of the main rotor is about 4.5 Hz; the model is integrated in time using an implicit A/L stable multistep scheme with tunable algorithmic dissipation, with a time step of 2 ms, corresponding to about 110 steps per revolution.

4 COUPLED BIOAEROSERVOELASTIC MODEL

In previous analyses (e.g. in [6, 22–24]) the BDFT of the pilot was modeled using transfer functions (e.g. those proposed by Mayo [7], or the functions identified by the authors in previous test campaigns [9]). In the following, the proposed detailed multibody model of the pilot's arm is directly coupled to the multibody model of the helicopter to assess the feasibility of integrated bioaeroservoelastic simulations. The essential changes consisted in connecting both the shoulder attachment point and the hinge of the collective control device to the finite element model of the helicopter's airframe, and in passing the collective control rotation as input to the flight control system. In the current analysis, both points are rigidly connected to a set of FE nodes in correspondence to the location of the pilot's seat, as no further detailed geometric and modal information about the cockpit layout was available. The rotation of the control device about its hinge is scaled using the gearing ratio GG_c and mixed to the output of the autopilot, to produce the desired command to the swashplate actuators.

Figure 11 contains the results obtained with the coupled model while performing a vertical maneuver inspired by the 'Rotorcraft handling qualities performance design specification' ADS-33 [27]. The maneuver consists in reducing the altitude of a helicopter of 75 ft (about 23 m) from hover as quickly as possible, reaching steady hover at the new altitude. The tracking of the desired trajectory (labeled 'ref' in the figure) is obtained using a simple model of the intentional pilot's behavior, $H_{\mathrm{ap}}(s)$, based on the crossover model [28], with a feedforward contribution [23]. The model of the pilot's intentional behavior, $H_{\mathrm{ap}}(s)$, stems from the consideration that the loop transfer function $H_L(s)$, consisting of the product between the pilot model and a model of the vehicle in the neighborhood of the crossover frequency ω_c, resembles an integrator with a time delay,

$$H_L(s) = H_{\mathrm{ap}}(s)H_{z\theta}(s) = \frac{\omega_c}{s}\mathrm{e}^{-\tau_e s}. \tag{9}$$

Such model of the pilot's intentional behavior is used to close an additional control loop. The collective pitch

$$\theta_0 = \theta_{\mathrm{ap}} + \theta_{\mathrm{ff}} + GG_c\psi \tag{10}$$

is thus made of two contributions: a voluntary part, θ_{ap}, which includes some form of feedforward $\theta_{\mathrm{ff}} = \hat{H}_{z\theta}^{-1}(s)z_d$ for the desired altitude z_d, where $\hat{H}_{z\theta}^{-1}(s)$ is the inverse

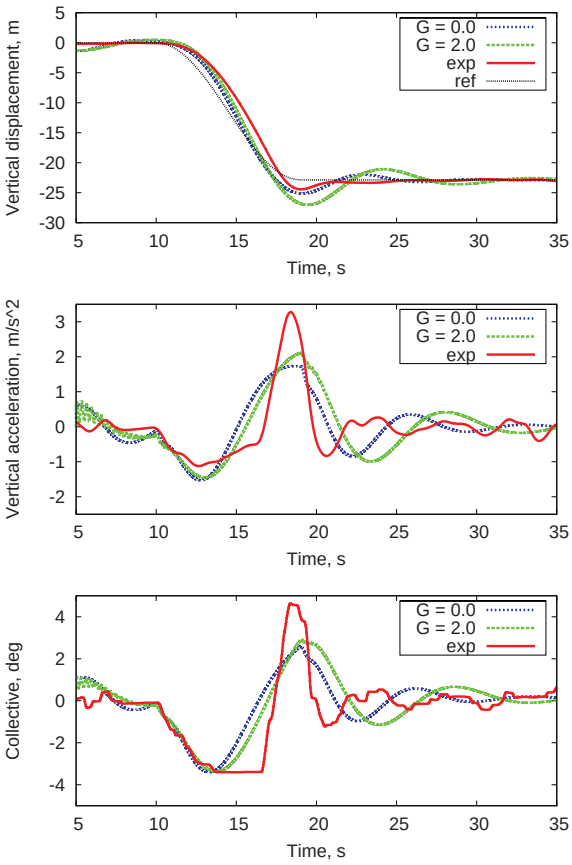

Fig. 11. Vertical maneuver: vertical displacement (top), acceleration (mid), and collective control rotation (bottom).

of the vehicle transfer function, low-pass filtered to become strictly proper, and an involuntary part, consisting of the control inceptor rotation ψ, caused by the BDFT, and scaled by the gearing ratio, G_c. The active part, θ_{ap}, is modeled using McRuer's crossover model [28]. The output of the vehicle model is thus

$$z = H_{z\theta}(s)\left(H_{ap}(s)(z_d - z) + \hat{H}_{z\theta}^{-1}(s) z_d + G G_c H_{BDFT} s^2 z\right), \tag{11}$$

i.e.

$$\left(1 + H_{z\theta}\left(H_{ap} - G G_c H_{BDFT} s^2\right)\right) z = H_{z\theta}\left(H_{ap} + \hat{H}_{z\theta}^{-1}\right) z_d. \tag{12}$$

In the direct multibody simulation, functions H_{ap} and $\hat{H}_{z\theta}^{-1}$ are realized in the time domain in state-space form, whereas the role of function H_{BDFT} is played by the proposed biomechanical model of the pilot's arm, and that of function $H_{z\theta}$ is played by the detailed multibody model of the helicopter.

Two models are considered in the plots of Fig. 11. They differ by the scaling factor that multiplies the involuntary pilot's input, resulting from the BDFT, and the signal that is actually input in the control system. The nominal value is used when $G = 1$. The plots illustrate the cases of $G = 0$ (negligible BDFT: unrealistic, but used as limit case) and $G = 2$ (twice the nominal value).

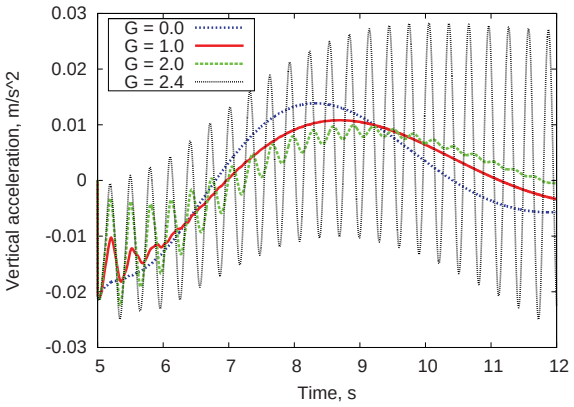

Fig. 12. Vertical acceleration of helicopter center of mass in hover.

For $G = 2$ the acceleration of the vehicle shows some oscillations at the frequency of the coupled bioaeroservoelastic mode when the collective control moves sharply. These oscillations are not present when $G = 0$.

The coupled system becomes unstable for $G = 2.4$, as shown in Fig. 12. The unstable mode corresponds to a rotor coning mode excited by collective pitch rotation caused by the oscillation of the pilot's arm, associated with appreciable vertical displacement of the helicopter. Several frames of the motion of the main rotor are shown in Fig. 13, after the unstable motion has developed into a limit cycle oscillation. For $G = 2$ the frequency of the coupled bioaeroservoelastic mode is about 3.4 Hz, with 7% of the critical damping. For $G = 2.4$ the frequency is 3.3 Hz, with -0.4% of the critical damping. Frequency and damping have been estimated by extracting proper orthogonal modes from the free response of the multibody analysis using the procedure described in [29]. A collective bounce instability with a gearing factor of more than twice the nominal value is consistent with similar results reported in [24] for a different rotorcraft and the BDFT transfer function proposed by Mayo [7].

Although the experimental and the numerical curves refer to different cases (the helicopter dynamics in the flight simulator was rather simplified, and related to a different vehicle model), the plots show a clear resemblance.

5 CONCLUSIONS

This work presented the application of a detailed biomechanical model of a helicopter pilot's arm to the bioaeroservoelastic analysis of involuntary adverse rotorcraft-pilot couplings. The arm model has been first

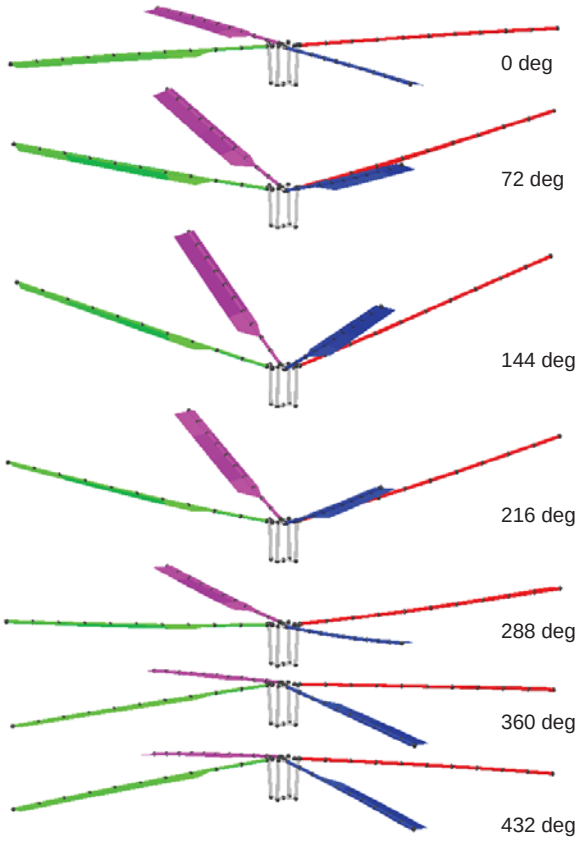

Fig. 13. Frames of main rotor motion taken at azimuth increments of 72 deg during a cycle of collective bounce oscillation after the instability developed into a limit cycle oscillation.

used to produce neuromuscular admittance and biodynamic feedthrough frequency response data. These results qualitatively resemble analogous experimental data available from the open literature. The direct analysis of the coupled system provides the analyst the unique capability to evaluate the sensitivity of complex aeromechanical systems to the biomechanical properties of the pilot.

Achnowledgements

The authors gratefully acknowledge the contribution of Andrea Zanoni to the development of the biomechanical model of the pilot, and of Domenico Capobianco to the analysis of the coupled pilot-vehicle model. The research leading to these results has received funding from the European Community's Seventh Framework Programme (FP7/2007–2013) under grant agreement N. 266073.

References

[1] Zanoni, A., Masarati, P., and Quaranta, G., 2012, "Rotorcraft pilot impedance from biomechanical model based on inverse dynamics," *International Mechanical Engineering Congress & Exposition (IMECE) 2012*, Houston, Texas, Paper No. IMECE2012-87533.

[2] Masarati, P., Quaranta, G., and Zanoni, A., in press, "Dependence of helicopter pilots' biodynamic feedthrough on upper limbs' muscular activation patterns," Proc. IMechE Part K: J. Multi-body Dynamics, doi:10.1177/1464419313490680.

[3] Venrooij, J., Abbink, D. A., Mulder, M., van Paassen, M. M., and Mulder, M., 2010, "Biodynamic feedthrough is task dependent," *2010 IEEE International Conference on Systems Man and Cybernetics (SMC)*, Istanbul, Turkey, pp. 2571–2578, doi:10.1109/ICSMC.2010.5641915.

[4] McRuer, D. T., 1997, *Aviation Safety and Pilot Control: Understanding and Preventing Unfavourable Pilot-Vehicle Interactions*, Washington DC: National Research Council, National Academy Press.

[5] Dieterich, O., Götz, J., DangVu, B., Haverdings, H., Masarati, P., Pavel, M. D., Jump, M., and Gennaretti, M., 2008, "Adverse rotorcraft-pilot coupling: Recent research activities in Europe," *34th European Rotorcraft Forum*, Liverpool, UK.

[6] Serafini, J., Gennaretti, M., Masarati, P., Quaranta, G., and Dieterich, O., 2008, "Aeroelastic and biodynamic modeling for stability analysis of rotorcraft-pilot coupling phenomena," *34th European Rotorcraft Forum*, Liverpool, UK.

[7] Mayo, J. R., 1989, "The involuntary participation of a human pilot in a helicopter collective control loop," *15th European Rotorcraft Forum*, Amsterdam, The Netherlands, pp. 81.1–12.

[8] Jump, M., Hodge, S., DangVu, B., Masarati, P., Quaranta, G., Mattaboni, M., Pavel, M. D., and Dieterich, O., 2008, "Adverse rotorcraft-pilot coupling: Test campaign development at the university of Liverpool," *34th European Rotorcraft Forum*, Liverpool, UK.

[9] Masarati, P., Quaranta, G., and Jump, M., 2013, "Experimental and numerical helicopter pilot characterization for aeroelastic rotorcraft-pilot couplings analysis," Proc. IMechE, Part G: J. Aerospace Engineering, **227**(1), pp. 124–140, doi:10.1177/0954410011427662.

[10] Venrooij, J., Yilmaz, D., Pavel, M. D., Quaranta, G., Jump, M., and Mulder, M., 2011, "Measuring biodynamic feedthrough in helicopters," *37th European Rotorcraft Forum*, Gallarate, Italy, pp. 199.1–12.

[11] Xiang, Y., Chung, H.-J., Kim, J. H., Bhatt, R., Rahmatalla, S., Yang, J., Marler, T., Arora, J. S., and Abdel-Malek, K., 2010, "Predictive dynamics: an optimization-based novel approach for human motion simulation," Structural and Multidisciplinary Optimization, **41**(3), pp. 465–479, doi:10.1007/s00158-009-0423-z.

[12] Xiang, Y., Arora, J. S., Rahmatalla, S., Marler, T., Bhatt, R., and Abdel-Malek, K., 2010, "Human lifting simulation using a multi-objective optimization approach," Multibody System Dynamics, **23**(4), pp. 431–451, doi:10.1007/s11044-009-9186-y.

[13] Pasciuto, I., Valero, A., Ausejo, S., and Celigüeta, J. T., 2011, "A hybrid dynamic motion prediction method with collision detection," *Proc. First International Symposium on Digital Human Modeling*.

[14] Xiang, Y., Arora, J. S., Chung, H.-J., Kwon, H.-J., Rahmatalla, S., Bhatt, R., and Abdel-Malek, K., 2012, "Predictive simulation of human walking transitions using an optimization formulation," Structural and Multidisciplinary Optimization, **45**(5), pp. 759–772, doi:10.1007/s00158-011-0712-1.

[15] Xiang, Y., Arora, J. S., and Abdel-Malek, K., 2012, "Hybrid predictive dynamics: a new approach to simulate human motion," Multibody System Dynamics, **28**(3), pp. 199–224, doi:10.1007/s11044-012-9306-y.

[16] Muscarello, V., Masarati, P., and Quaranta, G., 2012, "Multibody analysis of rotorcraft-pilot coupling," *2nd Joint International Conference on Multibody System Dynamics*, P. Eberhard and P. Ziegler, eds., Stuttgart, Germany.

[17] Pennestrì, E., Stefanelli, R., Valentini, P. P., and Vita, L., 2007, "Virtual musculo-skeletal model for the biomechanical analysis of the upper limb," Journal of Biomechanics, **40**(6), pp. 1350–1361, doi:10.1016/j.jbiomech.2006.05.013.

[18] Stroeve, S., 1999, "Impedance characteristics of a neuromusculoskeletal model of the human arm I. posture control," Biological Cybernetics, **81**(5–6), pp. 475–494, doi:10.1007/s004220050577.

[19] Stroeve, S., 1999, "Impedance characteristics of a neuromusculoskeletal model of the human arm II. movement control," Biological Cybernetics, **81**(5–6), pp. 495–504, doi:10.1007/s004220050578.

[20] Quaranta, G., Masarati, P., and Venrooij, J., 2013, "Impact of pilots' biodynamic feedthrough on rotorcraft by robust stability," Journal of Sound and Vibration, **332**(20), pp. 4948–4962, doi:10.1016/j.jsv.2013.04.020.

[21] Quaranta, G., Tamer, A., Muscarello, V., Masarati, P., Gennaretti, M., Serafini, J., and Colella, M. M., in press, "Rotorcraft aeroelastic stability using robust analysis," CEAS Aeronaut. J., doi:10.1007/s13272-013-0082-z.

[22] Masarati, P., Quaranta, G., Gennaretti, M., and Serafini, J., 2010, "Aeroservoelastic analysis of rotorcraft-pilot coupling: a parametric study," *American Helicopter Society 66th Annual Forum*, Phoenix, AZ.

[23] Masarati, P., Quaranta, G., Gennaretti, M., and Serafini, J., 2011, "An investigation of aeroelastic rotorcraft-pilot interaction," *37th European Rotorcraft Forum*, Gallarate, Italy, Paper no. 112.

[24] Gennaretti, M., Serafini, J., Masarati, P., and Quaranta, G., in press, "Effects of biodynamic feedthrough in rotorcraft-pilot coupling: the collective bounce case," J. of Guidance, Control, and Dynamics, doi:10.2514/1.61355.

[25] Bousman, W. G., Young, C., Toulmay, F., Gilbert, N. E., Strawn, R. C., Miller, J. V., Maier, T. H., Costes, M., and Beaumier, P., 1996, "A comparison of lifting-line and CFD methods with flight test data from a research Puma helicopter," TM 110421, NASA.

[26] Pitt, D. M. and Peters, D. A., 1981, "Theoretical prediction of dynamic-inflow derivatives," Vertica, **5**(1), pp. 21–34.

[27] Anonymous, 2000, "Performance specification, handling qualities requirements for military rotorcraft," ADS 33-E-PRF, US Army AMCOM, Redstone, Alabama.

[28] McRuer, D. T. and Jex, H. R., 1967, "A review of quasi-linear pilot models," Human Factors in Electronics, IEEE Transactions on, **HFE-8**(3), pp. 231–249, doi:10.1109/THFE.1967.234304.

[29] Quaranta, G., Masarati, P., and Mantegazza, P., 2004, "Assessing the local stability of periodic motions for large multibody nonlinear systems using POD," Journal of Sound and Vibration, **271**(3–5), pp. 1015–1038, doi:10.1016/j.jsv.2003.03.004.